Journal of Energy Storage 43 (2021) 103213

Contents lists available at ScienceDirect

Journal of Energy Storage

journal homepage: www.elsevier.com/locate/est

Experimental investigation of the failure mechanism of 18650 lithium-ion batteries due to shock and drop

Markus Spielbauer [a,b,*], Philipp Berg [b], Jonas Soellner [b], Julia Peters [c], Florian Schaeufl [a], Christian Rosenmüller [a], Oliver Bohlen [a], Andreas Jossen [b]

[a] Department of Electrical Engineering and Information Technology, Munich University of Applied Sciences, Lothstr. 64, 80335 Munich, Germany
[b] Institute for Electrical Energy Storage Technology, Technical University of Munich, Arcisstr. 21, 80333 Munich, Germany
[c] TÜV SÜD Battery Testing GmbH, Daimlerstr. 15, 85748 Garching, Germany

ARTICLE INFO

Keywords:
18650 lithium-ion battery safety
Mechanical abuse test
Vibration
Shock and drop
Failure mechanism
Current interruptive device

ABSTRACT

This work presents an experimental investigation of the failure mechanism of 18650 lithium-ion batteries subject to dynamic mechanical loads and the implications of severe damages on the safety function of the current interruptive device (CID), as current literature offers no insight in this topic. First, a conducted shock test series with loads beyond automotive standards showed no distinct impact on various modern cell types in impedance and computed tomography (CT) analysis, while older cell types exhibited signs of damage such as mandrel displacement and increase of ohmic resistance, as had already been reported in literature. A following investigation with acceleration measurements of drops of power tool battery modules revealed that accelerations in some applications can exceed even high load-level standards significantly. In a subsequent test series with axial drop tests in both orientations with various cell types, impact surfaces and states of charge (SOC), multiple cell types exhibited high ohmic failure without a thermal event. Computed Tomography (CT) and Post Mortem analysis revealed that, among various observable damage mechanisms, the predominant failure mechanism is contact loss in the CID region. Even severe mechanical damages, although influencing electrical and thermal behavior, showed no impact on the functionality of the CID in overcharge tests

1. Introduction

In many applications such as industrial use, power tools or mobility, cylindric 18650 lithium-ion battery cells are used as they offer high energy densities, are inexpensive, widely available and allow flexible module design. In these and other operational areas, the cells can be subject to severe mechanical loads from shocks, drops or vibration. As such load types are believed to be potential causes of catastrophic failure in battery packs and pose a risk to the safety of users and the environment, great effort is put into the testing of battery cells according to various standards and regulations [1] to ensure their safety during operation and into robust battery pack design to mitigate external loads on the cells [2].

Automotive test standards for lithium-ion batteries such as the SAE J2464 or SAE J2929 test small cells below 0.5 kg with repeated shocks with 150 g (not an SI unit but widely used in relevant literature, 1 g equates to 9.81 m/s^2) peak acceleration and a pulse duration of 6 ms in multiple directions, while larger cells generally have to withstand smaller loads [8,9]. Other automotive standards apply even smaller loads. The commonly used standard UN 38.3 [10] for the transport of dangerous goods recommends shock testing similar to the SAE J2464. [1,17,18].

For space applications, NASA/TM-2009-215751 recommends pyro shock testing of lithium-ion batteries from 20 g at 100 Hz up to 2000 g peak acceleration above 1.6 kHz [12]. The military standard MIL-STD-202G, not for lithium-ion batteries but for electronic and electronic and electrical component parts in general, defines different test levels up to 1500 g peak acceleration with 0.5 ms half-sine pulses. [11]

More general standards for shock testing such as the IEC 60068-2-27 define a range of severity levels for shock tests with peak accelerations up to 3000 g [13]. The same standard presents an overview of typical shock forms and loads from 15 g for stationary or shock-protected devices during transport up to 1500 g for semiconductors or microcircuits. A summary of commonly applied standards for shock tests is depicted in Table 1.

Drop tests, for example in the UL 2580 [6] or in the Freedom-CAR [15], are usually free fall tests from a wide range of heights up to

* Corresponding author at: Department of Electrical Engineering and Information Technology, Munich University of Applied Sciences, Lothstr. 64, 80335 Munich, Germany.
E-mail address: markus.spielbauer@hm.edu (M. Spielbauer).

https://doi.org/10.1016/j.est.2021.103213
Received 15 March 2021; Received in revised form 26 July 2021; Accepted 1 September 2021
Available online 24 September 2021

Table 1
Overview of shock test standards and regulations for small format battery cells and other components [1].

Standard	Application	Orientation	Number of Shocks	Peak Acceleration	Pulse width
UN/ECE-R100.02 [3]	Automotive	longitudinal, lateral	Either positive or negative direction or both	20–28 g, 8–15 g	80–120 ms
IEC 62660-2(3) [4]	Automotive	Analog to vehicle, all if unknown	10 per direction	51 g	6 ms
ISO 16750-3 [5]	Automotive	Analog to vehicle, all if unknown	10 per direction	51 g	6 ms
UL 2580 [6]	Automotive	3 axes	3 shocks in each direction, total 18	25 g	15 ms
UL 1642 [7]	Lithium batteries	3 axes, 2 for symmetry	3 shocks in each direction	125–175 g	75 g average in first 3 ms
SAE J2464 [8]	Automotive	3 axes	3 shocks in each direction, total 18	150 g	6 ms
SAE J2929 [9]	Automotive	longitudinal, lateral	One repetition each in positive and negative direction	150 g	6 ms
UN 38.3 [10]	Transportation	3 axes	3 shocks in each direction, total 18	150 g	6 ms
MIL-STD-202G [11]	Military, electrical component parts	3 axes	3 shocks in each direction, total 18	up to 1500 g	at 0.5 ms
NASA/TM-2009-215751 [12]	Space applications	3 axes	2 shocks in each direction	20–2000 g	Pyro-Shock, 0.1–10 kHz
IEC 60068-2-27 [13]	General	3 axes	3 shocks in each direction, total 18	up to 3000 g	At 0.2 ms

Table 2
Overview of drop test standards and regulations for battery cells and other components [1].

Standard	Application	Drop height	Impact surface
UL 2580 [6]	Automotive	1 m	Flat concrete surface
ISO 16750-3 [5]	Automotive	1 m	Concrete ground or steel plate
QC/T 743 [14]	Automotive	1.5 m	Hardwood floor
FreedomCAR [15]	Automotive	10 m	Steel object
MIL-STD-810H [16]	Military, Logistic transit	1.22 m	Steel backed by concrete

10 m with various impact surfaces and number of repetitions as shown in Table 2. [1]

While testing according to standards is necessary for quality control, it does not promote a better understanding of the underlying failure mechanisms, as they define simple evaluation criteria such as “no leakage, no venting, no disassembly, no rupture and no fire" or no drop in open-circuit voltage (OCV) larger than 10% [10]. With a wide range of peak accelerations defined in different standards for shock tests, for many applications, it is also unclear what the actual loads are that lithium-ion batteries are subjected to. Apart from this, there is also no information available, in which magnitude the loads occurring in drop tests are in comparison to shock tests.

Scientific literature offers more profound investigations regarding shocks and drops, but the number of available publications is relatively small. Brand et al. [19] used the pulse shape as defined in the UN38.3 to shock 18650 and pouch cells, but rather than applying 3 shocks for each axis, they conducted 300 in the axial direction. Despite this, they reported no significant changes in capacity or ohmic resistance or damage to the electrodes. For the 18650 cells, deformation of the current interruption device (CID) was observed, but it was not tested whether this deformation has negative effects on the functionality of the CID. Tsujikawa et al. [20] performed half-sine shock tests with 50 g peak acceleration and 11 ms pulse width in multiple orientations, as well as free-fall tests from up to 3 m height on large format cells and reported no leakage or voltage drop for either. Ebert et al. [21] applied automotive crash profiles with peak accelerations up to 45 g to 18650 and pouch cells and analyzed long-term cycling up to 80% state of health (SOH), for which they reported slightly accelerated aging for 18650 cells, while no significant changes were observed for the pouch cells.

More publications applying vibration tests than shock tests are available, whose results, even though vibrations are not investigated in this publication, are also concluded shortly here, as there is reason to assume that the potential failure mode is the same as for dynamic loads with higher accelerations.

Brand et al. [19] investigated vibrations with sine vibrations according to UN 38.3 and long-term sine sweep vibration in different orientations for 18650 and pouch cells. The pouch cells proved to be very resilient, and the tests of the 18650 cells showed no changes apart from a slight mandrel displacement in CT analysis either. Long-term vibration tests caused no cell failure but did cause increases in internal resistance, mandrel displacement, a partly melted separator and even a hole punched out in the negative pole by the mandrel for the 18650 cells. The authors suggested that this might cause the resistance increases but did not conclude a hypothesis about the ultimate failure mode.

Hooper and Bruen et al. [22,23] applied various load profiles to 18650 cells in different orientations and at various SOCs. No cell failures were observed, but for some of the tested cells they reported an increase in ohmic resistance, which they attributed to increasing contact resistance or delamination, but without further investigating the actual reason for this behavior or their implications on cell safety. Another study by Hooper et al. [24] on a different cell type with multi-axis vibration type presents similar results but with significantly smaller increases of ohmic resistance. Somerville [25] from the same research group attributed power and capacity loss from vibration to the damaging of boundary layers by analyzing electrolyte-deposited products after vibration testing. However, this publication does not conclude which mechanism will ultimately lead to cell failure either.

Berg et al. [26] tested the durability of 18 types of 18650 cells with different pre-cycling conditions various random vibration profiles and reported no degradation in resistance or capacity for any of the cells. For some cells with mandrel, CT scans revealed imprints of the mandrel in the anode current collectors, as had already been reported by Brand et al. [19]. As potential failure mechanisms, high ohmic failure due to contact loss as well as cut-out particles of the current collectors causing internal short circuits (ISCs) were assumed, but without being able to confirm or evaluate the probability of such events.

To conclude, neither standards nor literature offers a clear insight into the failure mode of lithium-ion batteries when undergoing critical mechanical load from shocks, drops or vibrations. On top of this, it is unclear if severe damages which do not cause an instantaneous event might harm the safety functions of the cells. However, such knowledge could be valuable, for example, for researchers investigating dynamic loads on battery cells or for cell manufacturers, who are still unaware of the predominant failure mode and who could thereby improve the cell design of upcoming cell generations. Also, companies using 18650 batteries in rough environments could benefit from such knowledge, as it makes a significant difference to safety requirements if cells drop out high ohmic or if they pose the threat of causing thermal runaways after undergoing severe shocks or vibrations. Moreover, information on the dominating failure mechanism is important for modeling of battery deterioration and research on possible fault-detection and prognosis.

For this reason, this paper investigates the failure mode of 18650 commercial lithium-ion batteries in dynamic load scenarios. Therefore, an experimental approach consisting of four successive steps, as depicted in Fig. 1, which also represents the structure of this paper, was chosen. As the steps are consecutive and to improve readability, each conducted test series is presented and discussed within the same section.

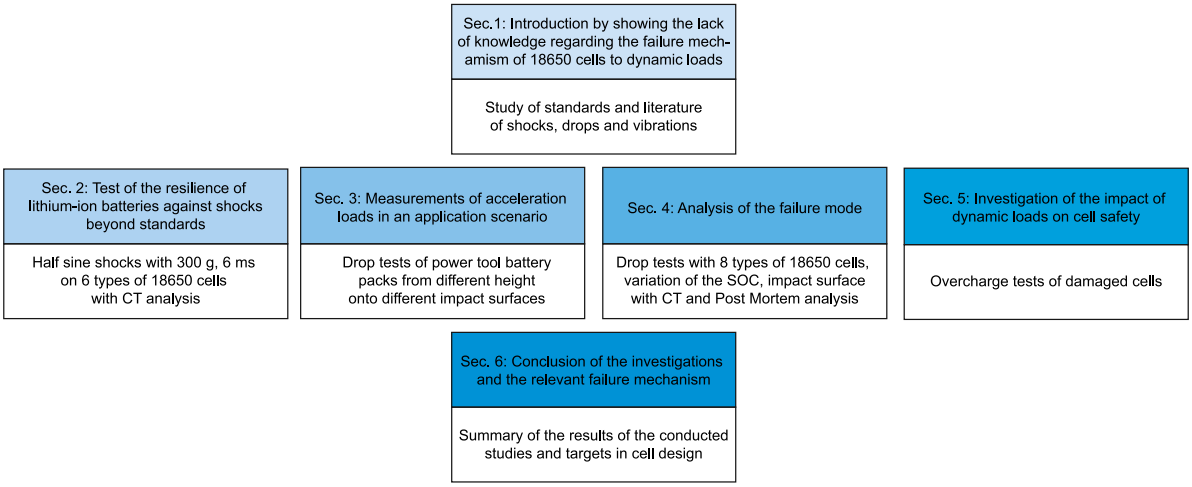

Fig. 1. Overview of the methodology applied in this paper to investigate the failure mode of 18650 lithium-ion battery cells.

2. Test of the resilience of lithium-ion batteries against shocks beyond transport standards

A first test series to investigate the resilience of lithium-ion batteries against shock and the relevant failure mode was performed by TÜV SÜD Battery Testing GmbH on a shock test machine.

2.1. Test setup

For this test series, a pneumatic shock test machine AVEX SM-110 by Benchmark Electronics Inc, as depicted in Fig. 2(a), was employed. The test machine is suitable for test specimens up to 90 kg and can be used to generate half-sine, sawtooth and square wave shocks using different pulse generator pads. For rigid fixation, the cells were mounted with M10 steel screws and 3D-printed cell holders.

To analyze the electrical behavior of the cells when undergoing shocks, electrochemical impedance spectroscopy (EIS) measurements were conducted before and after the tests. For this purpose, multiple Gamry Reference 5000P were used in galvanostatic mode with 100 mA AC RMS and a variable number of measurement points per decade with frequencies from 10 kHz to 1 Hz. Lower frequencies were not included as their measurement is very time-consuming, and the obtained results are strongly dependent on ambient temperature [27–30] and relaxation [31,32], making their evaluation questionable. Four-point sensing was enabled by cell holders from Battery Dynamics with spring probe pins, which allow fast and highly reproducible contacting.

To evaluate structural changes within the cells, µ-Computed Tomography (CT) scans were performed, with a phoenix nanotom s (GE Sensing & Inspection Technologies) at 130 kV and 120 µA with 2 × 2 binning, 18.3 µm voxel size, 3 averaged images for each projection and 1000 projections for every reconstruction. Rather than scanning the entire cell, each one scan of the positive and the negative pole was conducted. These settings allowed a short scan time with sufficient quality. The scans were evaluated with VGSTUDIO (Volume Graphics GmbH).

2.2. Performed tests

As cells are designed to withstand loads recommended by widely applied standards, for the first test series it was decided to exceed loads of automotive standards right away to increase the probability of provoking damage patterns, which is the purpose of this entire investigation. Therefore, instead of applying 150 g and 6 ms half-sine pulses, 300 g and 6 ms half-sine pulses were chosen. Also, the number of 1000 repetitions was chosen significantly above automotive

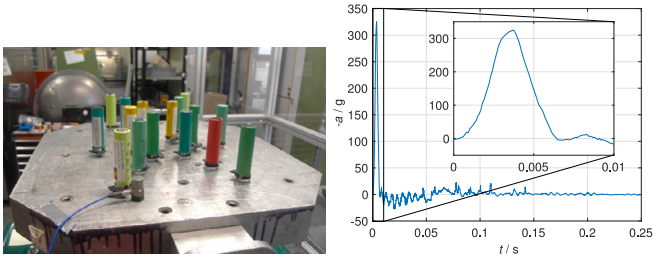

(a) Test setup with 16 cells of 6 different cell types for the half sine shocks on the acceleration and the foreground. **(b)** Pulse of a shock test with 300 g peak and 6 ms pulse width showing AVEX SM-110 with acceleration sensor in multiple secondary peaks.

Fig. 2. Test setup and pulse form for test series with half sine shocks.

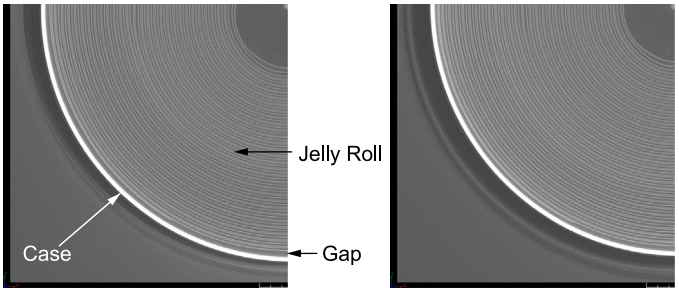

Fig. 3. CT-scans of pristine Samsung INR18650-25RM cell at 0% (left) and 100% (right) SOC showing a slightly larger gap between jelly roll and case at lower SOC. After multiple cycles this gap vanishes even at 0% SOC due to jelly roll swelling.

standards, which mostly do not exceed 3 repetitions per orientation. As cell orientation, axial shocks were chosen as in this direction more space for relative movement of the jelly roll is available, which was considered to bear a higher failure potential. For the verification of the pulse shape, the acceleration was measured by a single axis acceleration sensor 353B03 from PCB Piezotronics, which has a sensitivity of 10 mV/g, a measurement range of ± 500 g and a frequency range from 1 to 7000 Hz. The measurements were logged with a Q.bloxx A101 data logging system from Gantner Instruments. One verification measurement of a shock pulse is depicted in Fig. 2(b). While the main pulse shows a peak slightly above the desired 300 g, as well as multiple secondary pulses, the pulses are well within the acceptable variance recommended in typical standards [13].

Table 3
Cell types for the shock test with 300 g peak acceleration and 6 ms pulse width.

Cell type	Number of tested cells	Capacity	Max. charge current	Max. discharge current	Max. voltage	Min voltage	Mandrel
A123 APR18650M1-A	3	1.1 Ah	5 A	30 A	3.6 V	2.0 V	Yes
Moli IHR-18650-A	3	2.5 Ah	5 A	20 A	4.2 V	2.0 V	Yes
Panasonic UR18650-RX	1	2.05 Ah	1.435 A	10 A	4.2 V	2.75 V	No
"Samsung ICR18650-22F"	3	2.2 Ah	1 A	1 A	4.2 V	2.75 V	No
Samsung INR18650 25RM	3	2.5 Ah	4 A	20 A	4.2 V	2.5 V	No
Sony / Murata Konion US18650 VTC4	3	2.1 Ah	4 A	30 A	4.2 V	2.5 V	Yes

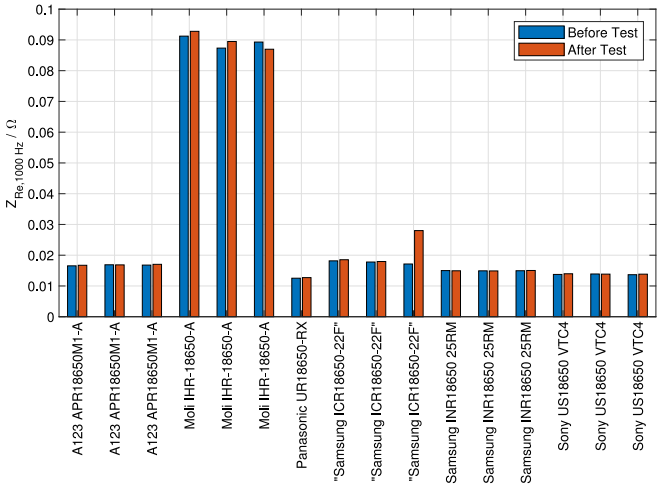

Fig. 4. Real part of the resistance at 1000 Hz before and after 1000 half sine shocks with 300 g and 6 ms pulse width.

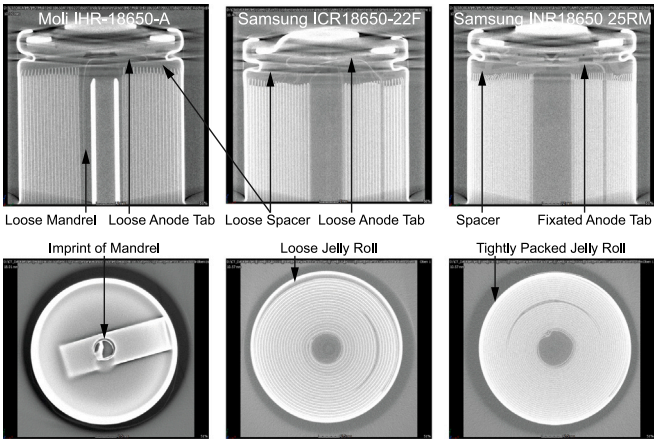

Fig. 5. CT-scans of the Moli IHR-18650-A, the Samsung IRC18650-22F and the Samsung INR18650 25RM after 1000 half-sine shocks with 300 g and 6 ms pulse width. The CT scans reveal insufficient fixation with spacers, loose anode tabs and loose packaging of the jelly roll for the Moli IHR-18650-A and the Samsung IRC18650-22F. The Moli IHR-18650-A shows an imprint of the loose mandrel. The Samsung INR18650 25RM shows no signs of damage due to its tight packaging and the use of spacers at both ends of the jelly roll.

For this first test, 6 cell types, in total 16 cells, were chosen as depicted in Table 3. Some of these cells represent state-of-the-art cell types, others are discontinued models as they had been used in the literature before [19]. Of these, the Samsung ICR18650-22F is shown in quotation marks, as it exhibits both different electric characteristics in the OCV and a varying inner cell structure from other 22F cells. This gives reason to assume that it is either non-authentic or a much older version of the cell (production code from 2011). Nevertheless, this cell type was included in this test, as it was considered a prime example of weak structural cell design and consequently more susceptible to mechanical damage. The tests were performed on pristine cells at 0% SOC, as it was suspected that the low jelly roll swelling and expansion of the graphite anode [33–35] would result in lower contact forces between the jelly roll layers and the case and more space for relative movement, as depicted in Fig. 3, making the cells more susceptible to shock-induced damages.

2.3. Results

During and after the shock test series, all cells remained electrically functional and none of the cells showed signs of ISCs or thermal events. The EIS measurements, conducted before and after the tests at 0% SOC without intermediate electrical load, exhibit only changes in the real part of the impedance. For this reason, Fig. 4 only depicts the real part of the impedance at 1000 Hz and not the entire impedance spectra, as the latter would offer no additional information. Most cells do not show any changes in their EIS spectrum. Merely, the discontinued Moli IHR-18650-A cells, as well as one of the presumably non-authentic Samsung ICR 18650-22F cells, showed a significant increase of ohmic resistance.

The CT analysis depicted in Fig. 5 revealed no signs of damages for most cells either. Only the Moli IHR-18650-A cells showed an imprint of the mandrel in the negative current collector, as had been observed in literature before [19,26]. The CT scans of the Samsung ICR 18650-22F showed no clear signs of damage but reveal the loose jelly roll and insufficient fixation in the upper and lower parts of the cell, which allows significant relative movement. State-of-the-art cells, like the Samsung INR18650 25RM, which is exemplarily depicted, are more tightly packed and have larger spacers in both the positive and negative pole directions to prohibit relative movement of the jelly roll and are therefore more resilient to shock loads.

2.4. Discussion

In this first investigation with loads beyond automotive test standards for 18650 cells, several damage mechanisms already known from literature could be observed for the older cell types, such as increases of ohmic resistance and imprints of loose mandrels, while state-of-the-art cells showed no indications of damages. Nevertheless, neither for older nor for state-of-the-art cell types, an ultimate failure occurred that would allow the assessment of the failure mode. At this point, the question arises, if loads beyond automotive test standards can occur in applications (and which acceleration levels they reach) and therefore if it even makes sense to investigate the failure mode at higher loads, or if further analysis of the failure mode can be relinquished.

3. Measurements of acceleration loads in an application scenario

To investigate if loads beyond typical standards and regulations occur and if the failure mode is even practically relevant, it was decided to measure accelerations in a use case. Therefore, as a high probability and high load scenario, drops of a battery pack used for power tool applications, as they might occur e.g. when dropped from scaffolds in construction sites, were investigated.

3.1. Test setup

For this reason, a drop tower with a pneumatic clutch system for increased reproducibility was developed, as depicted in Fig. 6(a). The

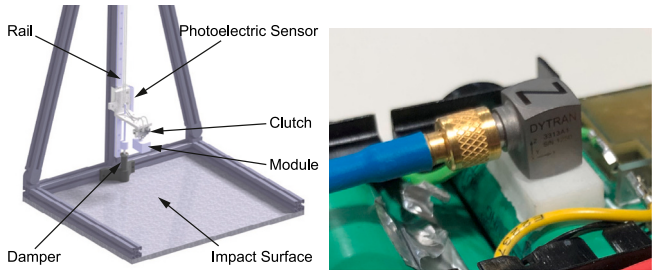

(a) Test bench for acceleration measurements in drop tests. A clutch system attached to a rail releases test objects before the impact triggered by a photoelectric sensor for increased reproducibility. **(b)** Acceleration sensor mounted on a cell of a commercial power tool battery pack. The case of the battery pack was removed for this picture.

Fig. 6. Test setup for acceleration measurements on cells and modules.

clutch system is attached to a rail, which guides the fall and allows holding the test object at a defined angle up until releasing it right before impact by triggering a photoelectric barrier. To cushion the shocks caused by the impact of the clutch, a hydraulic damper was attached to the end of the rail. Various impact surfaces can be mounted to the ground plate with screw joints.

To measure the occurring accelerations, a three axial acceleration sensor 3313A1 from Dytran, which has a sensitivity of 1 mV/g, a measurement range of ± 5000 g, a frequency range from 1.2 to 10000 Hz, a natural frequency > 30 kHz and a weight of 4.1 g, with a high-frequency data logger from National Instruments (NI 9232 BNC) with 3 channels and 102.4 kHz logging frequency was used with maximum logging frequency.

3.2. Performed tests

With this test bench, drop tests were performed on a commercial 4s2p battery module for power tools with 18650 cells and a total weight of 0.8 kg, yet without a power tool attached. To fixate the acceleration sensor on the module, an adapter was glued onto a cell, onto which the sensor was mounted by a screw joint, as depicted in Fig. 6(b), following recommendations in [36]. Due to the tight packaging of the battery module, a small hole had to be cut out of the module's case to create sufficient space for the sensor and the connecting cable. As drop heights, 0.5 m, 1.0 m, 1.5 m and 2.0 m were chosen, with aluminum and polyurethane (shore A hardness 90, thickness 5 mm) as impact surfaces. For the module drop tests, 15 repetitions were performed for each variation, of which the 10 tests showing least deviation were evaluated.

3.3. Results

For the quantification of the results of the drop tests, the peak acceleration values were evaluated. An overview of these is shown in Table 4.

The results of the drop tests on commercial power tool battery packs are exemplarily displayed for the shocks with 2.0 m fall height and impact on aluminum in Fig. 7(a) and for polyurethane in Fig. 7(b). The figures for all conducted drop tests are displayed in Fig. B.18. The tests show intricate pulse patterns with good repeatability before the first peak acceleration value but more deviations and long phases with high acceleration levels after the first peak. Additionally, multiple acceleration peaks with lower acceleration levels occur for secondary impacts, but these are not displayed in these plots as they are much later than visible on the applied time scale.

For the drop tests on polyurethane, the average measured peak accelerations ranged from 800 g in the 0.5 m drop up to 1611 g in the 2.0 m drop, while drops on aluminum ranged from 635 g to 2416 g, with the latter showing significantly larger deviations between the repetitions. It is noticeable that the resulting acceleration peak values are larger for the significantly harder aluminum surface for all tests except the 0.5 m drop test, for which the drops on the aluminum surface result in smaller peak values.

With this, it must be taken into consideration that not only the peak value but also the duration and shape of the shock pulse characterize the impact and that peak acceleration alone is not sufficient to precisely evaluate the severity of a drop test on its own. While it is difficult to assess the pulse durations due to their intricate form, at least for the first peak, durations in the magnitude of 1 ms can be estimated.

Table 4
Overview of average accelerations measured in drop tests on single cells and battery modules.

Drop height	Impact surface	Peak acceleration
0.5 m	Polyurethane	800 g
1.0 m	Polyurethane	1049 g
1.5 m	Polyurethane	1331 g
2.0 m	Polyurethane	1611 g
0.5 m	Aluminum	635 g
1.0 m	Aluminum	1177 g
1.5 m	Aluminum	1624 g
2.0 m	Aluminum	2416 g

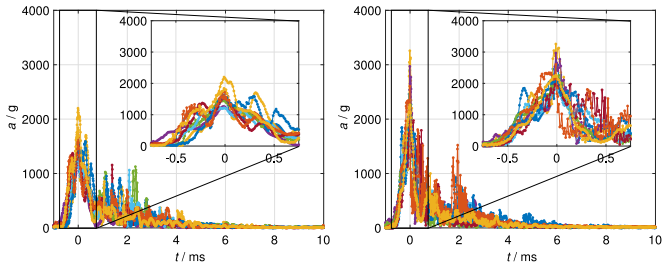

(a) Module drop onto polyurethane surface. **(b)** Module drop onto aluminum surface.

Fig. 7. Acceleration measurements of the impact of a power tool module from a 2.0 m drop. Each 10 repetitions are displayed in the plots.

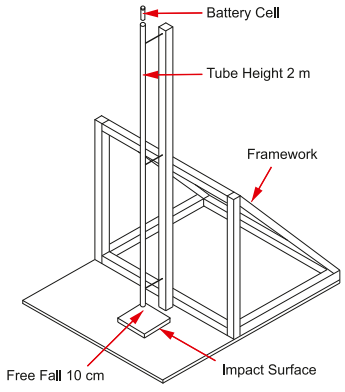

Fig. 8. Illustration of the test bench for guided drop tests with a 2.0 m long tube with diameter of 22 mm, 10 cm freefall before impact and exchangeable impact surfaces.

3.4. Discussion

The module drop test series has shown that the impact accelerations of drops from 2.0 m exceed automotive or transportation standards by far and with respect to acceleration also exceed the severe requirements that the NASA/TM-2009-215751 test standard recommends [12]-despite robust packaging with implemented damping components and without a power tool attached. Furthermore, even

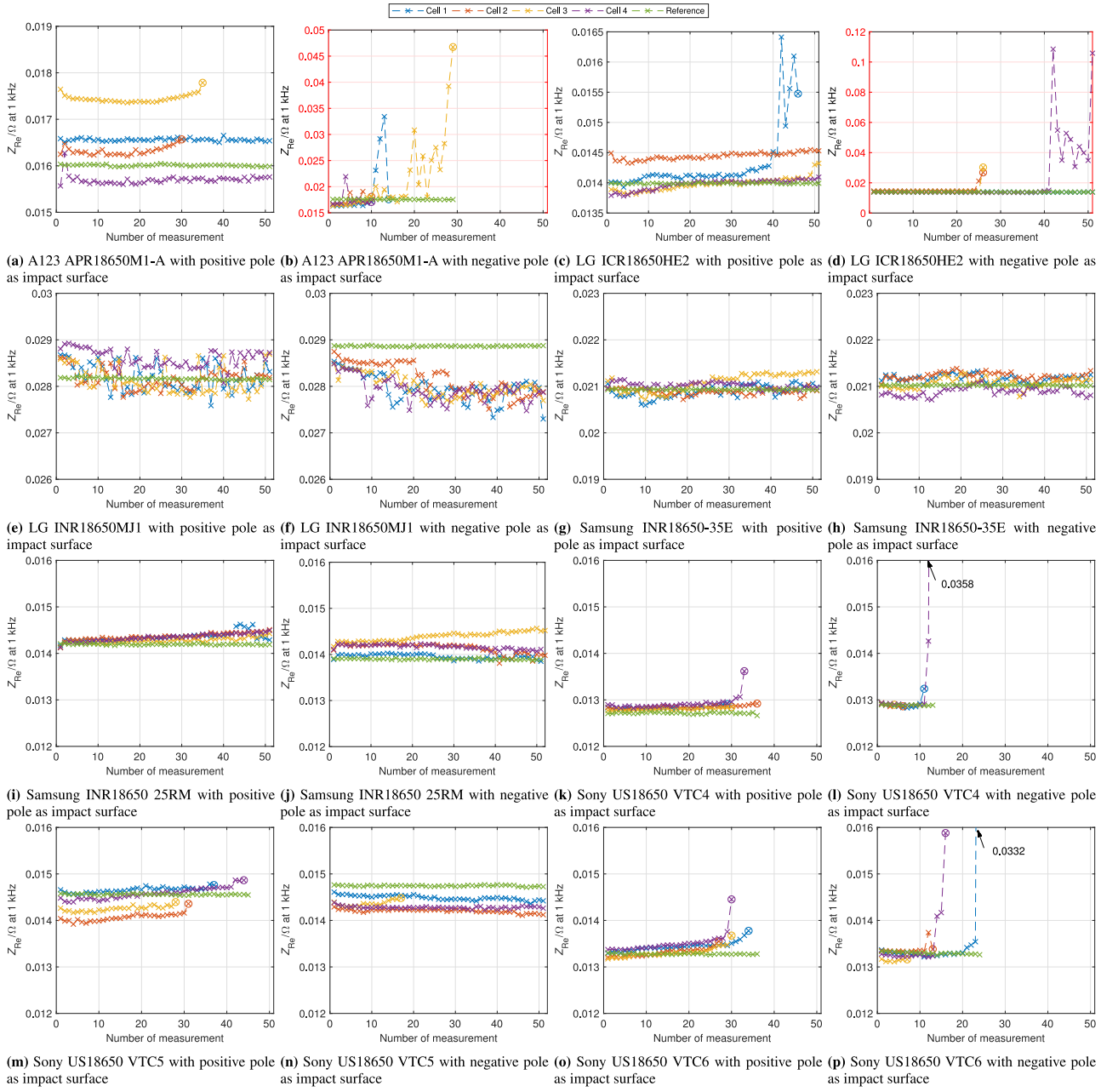

(a) A123 APR18650M1-A with positive pole as impact surface **(b)** A123 APR18650M1-A with negative pole as impact surface **(c)** LG ICR18650HE2 with positive pole as impact surface **(d)** LG ICR18650HE2 with negative pole as impact surface

(e) LG INR18650MJ1 with positive pole as impact surface **(f)** LG INR18650MJ1 with negative pole as impact surface **(g)** Samsung INR18650-35E with positive pole as impact surface **(h)** Samsung INR18650-35E with negative pole as impact surface

(i) Samsung INR18650 25RM with positive pole as impact surface **(j)** Samsung INR18650 25RM with negative pole as impact surface **(k)** Sony US18650 VTC4 with positive pole as impact surface **(l)** Sony US18650 VTC4 with negative pole as impact surface

(m) Sony US18650 VTC5 with positive pole as impact surface **(n)** Sony US18650 VTC5 with negative pole as impact surface **(o)** Sony US18650 VTC6 with positive pole as impact surface **(p)** Sony US18650 VTC6 with negative pole as impact surface

Fig. 9. Changes in the real part of the impedance at 1 kHz for the drop tests with 8 cell types onto aluminum. Cell failure is marked in the plots with a circle. Different *y*-axis scaling is marked red. (For interpretation of the references to color in this figure legend, the reader is referred to the web version of this article.)

deeper drops from more than 2.0 m are a plausible scenario, which additionally would result in even higher accelerations and could potentially cause battery failure. In this light, further investigation of the failure mode appears to be worthwhile and is proceeded in this paper.

Regarding battery abuse testing, it is highly recommended to measure the actual accelerations in the environment of the specific use case and to design battery tests based on the results rather than applying commonly used standards without considering the actual loads. To reliably detect such impacts, as it might be desirable for online detection in power tools, a measurement frequency of at least 5–10 kHz should be chosen.

4. Analysis of the failure mode

After determining that accelerations in use cases can exceed even severe standards and further testing with loads beyond typical standards is worthwhile, the following section presents an investigation of the failure mode by conducting repetitive drop tests in combination with CT scans and Post Mortem analysis.

4.1. Repeated drop tests on single cells to provoke cell failure

To provoke and analyze the failure mode of 18650 battery cells, a series of repeated drop tests with variations of the impact surface and the SOC are presented in the following section.

4.1.1. Test setup

As the achievable accelerations with the pneumatic shock tester turned out to be too low to provoke cell failure and thereby investigate the failure mechanism, further tests with this machine were relinquished. Instead, it was decided to continue the experimental investigations of the failure with drop tests, which cause significantly

Table 5
Cell types for the drop tests from 2.0 m.

Cell type	Capacity	Max. charge current	Max. discharge current	Max. voltage	Min voltage
A123 APR18650M1-A	1.1 Ah	5 A	30 A	3.6 V	2.0 V
LG ICR18650HE2	2.5 Ah	4 A	20 A	4.2 V	2.5 V
LG INR18650MJ1	3.5 Ah	4 A	10 A	4.2 V	2.5 V
Samsung INR18650-35E	3.4 Ah	8 A	13 A	4.2 V	2.65 V
Samsung INR18650 25RM	2.5 Ah	4 A	20 A	4.2 V	2.5 V
Sony / Murata Konion US18650 VTC4	2.1 Ah	4 A	30 A	4.2 V	2.5 V
Sony / Murata Konion US18650 VTC5	2.6 Ah	4 A	30 A	4.2 V	2.0 V
Sony / Murata Konion US18650 VTC6	3.12 Ah	5 A	15 A	4.25 V	2.0 V

higher accelerations and therefore have a higher chance of provoking the failure mode. Instead of conducting further tests on modules, a drop test bench for single cells was constructed, as this made the test procedure and the evaluation of the cells state during the tests easier and reduced the complexity of the load condition. Although commonly applied standards usually recommend free fall testing, a simple test stand with a 2.0 m tube (inner diameter 22 mm) mounted onto a wireframe was designed, as depicted in Fig. 8, to guide single cells during the fall and to enable improved repeatability. To achieve a well reproducible cell impact angle and undampened cell impact at the same time, it was decided to position the end of the tube 10 cm above the impact surface. This setup allowed the usage of different impact surfaces, which were fixated on the underlying surface to reduce bouncing. The tests were conducted in a room with temperature regulation at ~ 22 °C. To avoid any influence on the cell temperature due to their handling, gloves were used for all drop tests.

4.1.2. Performed tests

For the first set of drop tests, 8 different cell types (Table 5) were chosen due to their internal cell design (mandrel, tab configuration) [26] and repeatedly dropped on either their positive or negative pole on aluminum. Each 4 cells for the drop tests and 1 cell for reference were handled alike. Like the previous tests with the pneumatic shock tester, these experiments were performed on pristine cells at 0% SOC. Before the first and after each drop, an EIS measurement was performed at the same SOC until reaching 50 drops or until no more valid EIS measurement was possible for the cell.

In the second test series, the Samsung INR18650 25RM was dropped in negative pole direction onto the previously used, softer polyurethane surface until cell failure to investigate if the same failure mode occurs and to analyze if there are more distinct indicators of an imminent cell failure at lower loads.

The third set of drop tests was conducted on Sony/Murata Konion US18650 VTC6 cells, for reasons explained later, with the same setup as the first set of drop tests but a variation of the SOCs with 25%, 50%, 75% and 100% and impact on the positive pole only. As the batch of cells had a different production code than the cells tested beforehand, the test with 0% SOC cells was also repeated to analyze the repeatability of the test series.

4.2. Results

4.2.1. Drop tests with aluminum as impact surface

In the axial drop test series on aluminum with cells with 0% SOC, none of the cells showed indications of self-heating or any thermal event. Despite the severity of the shocks, which even lead to case deformation for the drop tests on the negative pole, all cells withstood at least 4 drop repetitions than was the case for the older cell type Sony US18650 VTC4 for the drop on the negative pole. Other cell types withstood substantially more shocks and some even the maximum of 50 drops.

As the changes of the impedance in this test series were primarily shifts of the real part of the impedance, the analysis in Fig. 9 depicts the real part of the impedance Z_{Re} at 1000 Hz of the cells measured

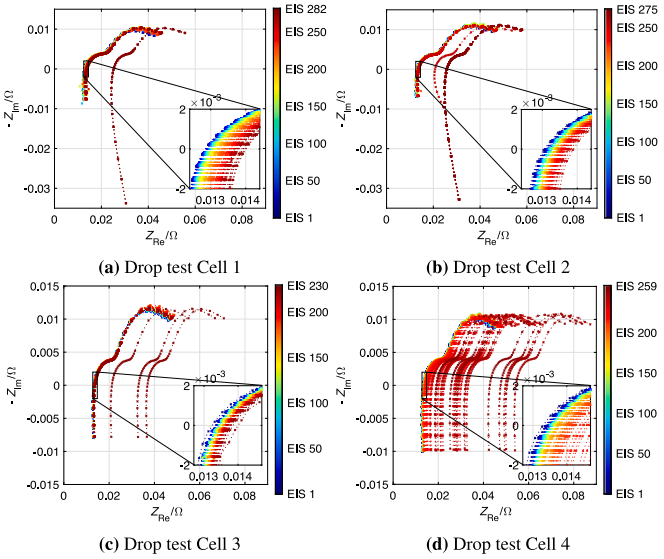

Fig. 10. Nyquist Plots for the Samsung INR18650 25RM cells dropped onto their negative pole on polyurethane after every drop test up until cell failure. (For interpretation of the references to color in this figure legend, the reader is referred to the web version of this article.)

during the shock tests and displays the numbers of drops until cell failure (no more EIS measurement possible) or up until 50 drops. A shorter overview of the results is presented in Table 6. Initial variations in ohmic resistance can be attributed to cell-to-cell variations [37,38] and measurement-related differences in the cables connecting the cell holders to the galvanostats, which influence the measurement despite four-channel sensing.

Some of the tested cell types, especially in Fig. 9(b), Fig. 9(d), Fig. 9(o) or Fig. 9(p), exhibit an increasing real part of the impedance before cell failure. This increase is little for some cells, but significant for others, like for cell 3 in Fig. 9(b), which shows almost a threefold increase in the real part of the impedance. Others such as Fig. 9(e) or Fig. 9(h) show distinct, yet small changes compared to the reference cells, but without a recognizable trend. Noticeable is that primarily the cell types that exhibit no cell failure are the ones that also show no increases in resistance. Nevertheless, these cells likely show an increase in ohmic resistance and the same failure mode when dropped more often, as was observed in a pre-test (depicted in Fig. C.19).

4.2.2. Drop tests with polyurethane as impact surface

In the drop tests with the Samsung INR18650 25 RM onto polyurethane on the negative pole at 0% SOC, the cells showed no signs of external case deformation and no signs of a thermal event. Cell failures occurred after 230 drops for the first and after 282 drop repetitions for the last cell.

The EIS measurements show progressive increases of the real part of the impedance for all tested cells, with up to four times the initial value up until cell failure. Cell 1 (Fig. 10(a)) and 2 (Fig. 10(b)) also

Table 6
Overview of failed cells for each cell type and changes in Z_{Re} at 1000 Hz for the failed cells at the last valid measurement and intact cells after 50 drops.

Cell Type	Cell Impact	Cells failed	Average ΔZ_{Re} with cell failure in $m\Omega$	Average ΔZ_{Re} without cell failure in $m\Omega$
A123 APR18650M1-A	Top	2	0.23	0.07
	Bottom	4	8.37	–
LG ICR18650HE2	Top	1	1.46	0.26
	Bottom	2	14.20	45.77
LG INR18650MJ1	Top	0	–	−0.19
	Bottom	0	–	−0.88
Samsung INR18650-35E	Top	0	–	0.02
	Bottom	0	–	0.14
Samsung INR18650 25RM	Top	0	–	0.29
	Bottom	0	–	0.05
Sony / Murata Konion US18650 VTC4	Top	4	0.23	–
	Bottom	4	5.79	–
Sony / Murata Konion US18650 VTC5	Top	4	0.23	–
	Bottom	1	0.09	−0.16
Sony / Murata Konion US18650 VTC6	Top	4	0.60	
	Bottom	4	5.63	–

show a shift for high frequencies in the inductive branch right before the cell failure. While cell 3 in Fig. 10(c) shows progressive increases in ohmic resistance, cell 4 in Fig. 10(d) shows progressive increases at first, but after reaching a high damage level (indicated by the darker red colors), the resistance exhibits volatile fluctuations without a recognizable pattern up until cell failure.

4.2.3. Drop tests with variation of the SOC

The drop test results of the SOC variation of the Sony/Murata Konion US18650 VTC6 are depicted in Fig. 11. The repetition of reference test at 0% SOC in Fig. 11(a) shows similar resilience of the cells as the tests on the same cell type with a different production code in Fig. 9(o), which indicates little difference between the cells with different production codes and good achievable reproducibility with the drop test setup.

Regarding the impact of the SOC on the resilience of 18650 cells towards shocks, the tests allow no conclusive assertion, yet indicate that cells, as assumed, fail slightly faster at lower SOCs. While for this test series none of the cells exhibited a thermal runaway either, at higher SOCs some of the cells, e.g. cell 4 for the variation at 100% SOC in Fig. 11(e), showed self-heating after multiple drops before the ultimate disruption of the current path. This can also be noticed in the decrease of the cell impedance, as well as in the Nyquist Plot of the test in Fig. 12(a), which displays a similar pattern as a cell on which a temperature variation was conducted in a climate chamber as depicted in Fig. 12(b). Their comparison indicates a temperature increase of 15–20 °C during the drop test.

4.3. CT and post mortem analysis to investigate the failure mode

While the EIS measurements during the drop tests showed increases in ohmic resistance right before cell failure, this observation does not allow direct assessment of the failure mode. Therefore, to improve the understanding of the failure mechanism, CT scans were performed and Post Mortem analysis was conducted.

4.3.1. CT analysis

For the drop tests on aluminum and polyurethane, CT scans of the Samsung INR18650 25RM conducted before and after the drop test series are depicted in Fig. 13. As the cells show similar damage patterns, the CT scans for the variation at 0% SOC can be found in Fig. D.20. The CT scans for the cells of SOC variation are not included as they show no differences in the observable damage patterns.

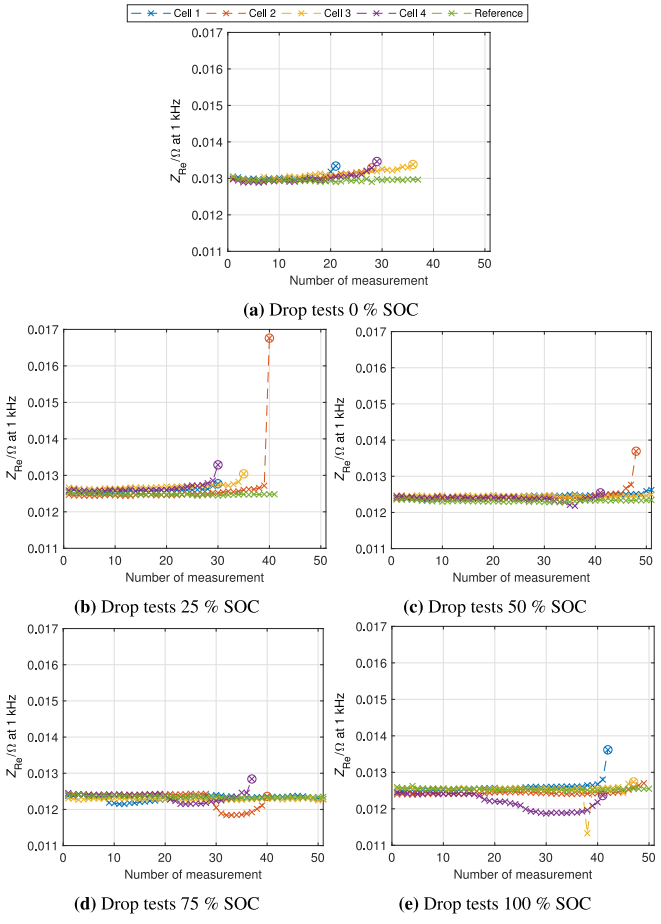

Fig. 11. Real part of the impedance at 1 kHz for the drop tests with SOC variation of the Sony/Murata Konion US18650 VTC6 of the positive pole onto aluminum measured after each drop. Cell failure is marked in the plots with a circle.

For the cells with impact on the positive pole onto the aluminum surface, severe CID deformation (depicted in Fig. D.20 green) can be observed, both for cell types with and without mandrel, as the load is transferred from the cap at the positive pole to the CID components. Additionally, relative jelly roll movement towards the positive pole with deformation of the overhanging anodes and separators in the area

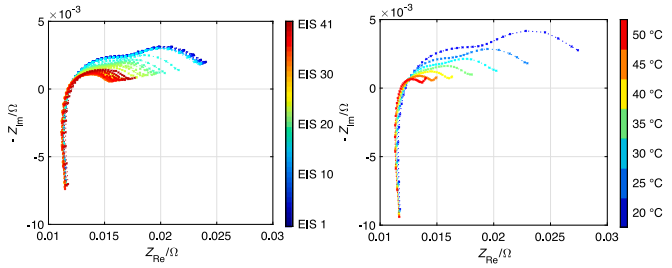

(a) Nyquist Plots of EIS measurements of cell 4 with 100 % SOC **(b)** Nyquist Plots of a temperature variation of a cell of the same type at 100 % SOC

Fig. 12. Comparison of Nyquist Plots of a Sony US18650 VTC6 cell with self-heating due to internal short circuit with a temperature variation of the same cell type.

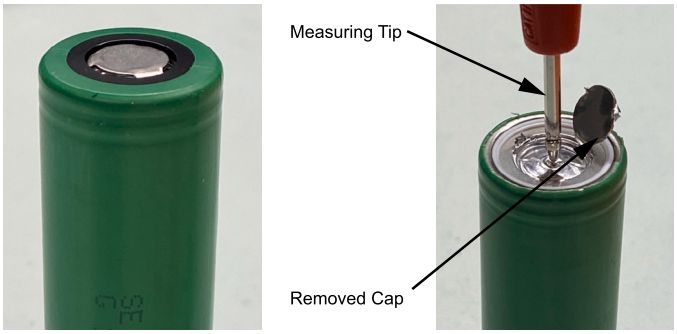

Fig. 14. Post Mortem analysis by removing the cap of the positive pole and applying pressure to the CID of a defunct cell.

of the casing bead and spacer deformation can be observed (depicted in Fig. D.20 red). This relative movement causes a similar damage pattern to the jelly roll as axial compression does [39,40]. For the cells with negative pole impact, case deformation and displacement of the jelly roll accompanied by deformation of the overhanging anodes and separators can be observed. Additionally, the negative tabs and inner jelly roll layers show significant deformation (Fig. D.20 blue). For the cell types with mandrels, imprints on the negative current collector tabs can be reported.

The cells dropped onto polyurethane show no external case deformation and no significant deformation of the CID, but significant jelly roll relative movement and deformation of the overhanging anodes and separators.

While the CT scans reveal clear signs of various damage mechanisms, they do not provide evidence of what ultimately makes the cells fail and interrupts the current path.

4.3.2. Post Mortem analysis

As analysis of the CT scans alone allowed no clear statement regarding the failure mechanism, Post Mortem analysis was conducted on the cells that failed in the drop test series in Section 4.2. Complete cell dismantling of a cell showed that the current path along the tabs was still intact for dysfunctional cells but allowed no clear statement regarding the current path in the positive or negative pole region as its mechanical integrity was destroyed during the dismantling process.

To further investigate if the current path in the pole regions was the reason for the cell failures, the caps from the positive pole were removed, as depicted in Fig. 14, to apply manual pressure with measuring tips to the CID. With this it was possible to measure the original cell voltages temporarily. After the exertion of more force, which lead to a slight deformation of the CID, the current path of the cells became permanently restored. This procedure was conducted for all failed cells, which revealed that the current path was restorable for all of them, which is a strong indicator that the primary failure mode for 18650 cells due to high dynamic loads is high ohmic contact loss in the CID region.

While none of the cells with 0% SOC showed any signs of temperature increase during the tests, this might not have been due to the absence of an internal short circuit, but due to the low energy content of the cells and small resulting heat generation in the case of such an event. For this reason, the cell voltage was measured after 3 months of storage. With this, a voltage drop > 0.1 V was chosen as an indicator of an ISC. However, it has to be mentioned that the voltage drop could also originate from a defect seal at the positive pole allowing air humidity to leak into the cell and thereby causing the voltage drop. According to this criterion, only three of the Sony/Murata Konion US18650 VTC6 cells that were dropped onto the positive pole showed signs of an ISC with voltage drops from 2.9 V to 2.70 V, 2.47 V and 2.07 V, which is also why this cell type was chosen for the test series with the SOC variation. A potential reason for the occurring short circuits for this cell type and deformation direction might be the jelly roll deformation in the area of the bead of cell case at the positive pole, as depicted in Fig. 15.

4.4. Discussion

The results of the drop tests onto aluminum at 0% SOC paired with the Post Mortem analysis confirmed that, while there were also other

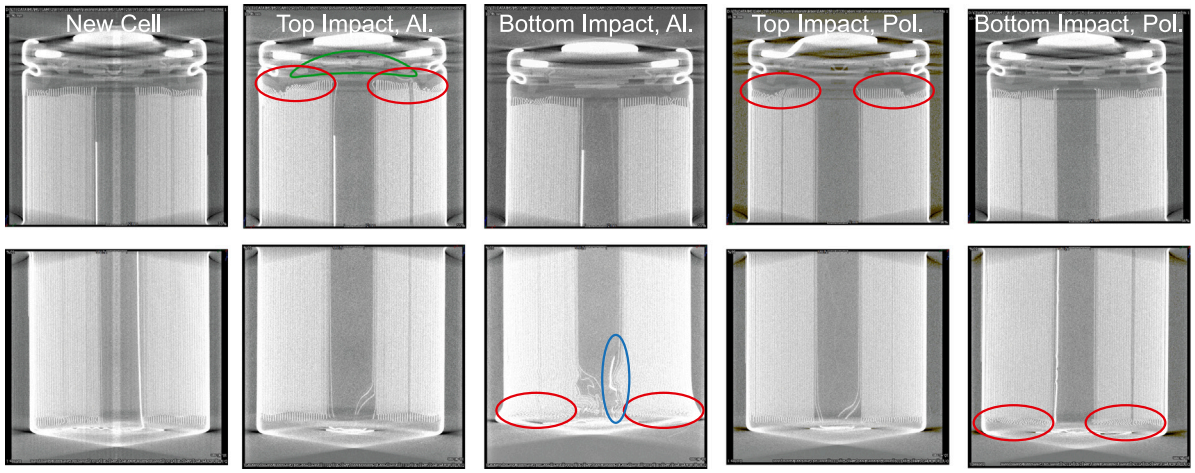

Fig. 13. CT Scans of the drop test with top and bottom impact of the Samsung INR18650 25RM on aluminum (Al.) and polyurethane (Pol.) at 0% SOC. Deformation of overhanging anode (red), the CID (green) and current collectors (blue) can be observed. All CT scans from drop tests with 0% SOC can be found in Fig. D.20. (For interpretation of the references to color in this figure legend, the reader is referred to the web version of this article.)

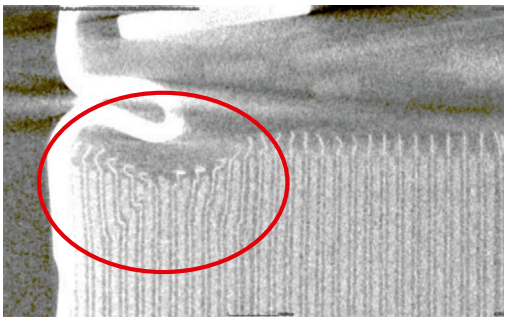

Fig. 15. CT scan of the deformation of the jelly roll for the test of the Sony/Murata Konion US18650 VTC6 with drop tests in the direction of the positive pole. The short anode and separator overhang and the consequentially reduced damping effect facilitates a strong deformation in the area of the cell case bead due to shocks.

damage mechanisms observable, the predominant failure mechanism of 18650 cells due to drop tests is contact loss in the CID region, as had already been assumed in literature [22,26].

For the conducted drop tests, this failure mode is often precedented by a progressive increase of ohmic resistance, which is the case for drops both on aluminum and polyurethane. Thereby, the latter is showing the progressive increase more clearly as a state of severe damage is not skipped over as often as in the more damaging drops onto aluminum. The fluctuations observed for some cells in Fig. 10(d) might indicate loose contact within the cells.

Despite the differences in the severity of the loads and even the increasingly deforming nature of the drop tests, the similarity in the rise of ohmic resistance in the EIS [19,22,24–26] gives reason to conjecture that the primary failure mechanism is the same for shocks and vibrations.

The EIS measurements indicate a related damage mechanism, as Figs. 10(a) and 10(b) show significant changes in the inductive branch of the Nyquist Plots right before cell failure. A potential explanation for this behavior could be a change in the current path, as Osswald et al. [41] observed similar shifts in impedance for measurements on a 26650 cell when selectively connecting some of the tabs. As not all cells have multiple anode and cathode tabs [26], this behavior cannot be expected from every cell type.

A further damage mechanism was observed in the SOC variation with the Sony/Murata Konion US18650 VTC6, which was deliberately conducted on the cell type as it also showed signs of ISCs at low SOC. For this cell, self-heating was observed before the failure of the CID, as shown in Fig. 12, but without causing a hazardous thermal runaway. The more distinct deformation of the jelly roll at the bead of the cell, which is likely the cause of the ISC, is especially severe for this cell type, as it has a particularly short anode and separator overhangs at the top (see Table E.8) and the bottom of the jelly roll, which act as dampening components. This is potentially a result of the reduction of dead mass and volume to increase the energy content or due to different electrode balancing. Either way, this cell design adjustment seems to conflict with the goal of cell safety.

Regarding the influence of the SOC on the resilience against drops, the test does not allow a definite statement due to the small sample size, yet indicates that the ultimate failure of the CID might occur slightly faster at lower SOCs. Such behavior could also be explained by the previously mentioned expansion of the anode at larger SOCs, which would result in smaller void spaces in the jelly roll for relative movement and higher contact forces between the jelly roll and the case. Therefore, another conflict of goals seems to be between enough space within the cell to compensate for jelly roll swelling and tight packaging to avoid relative movement.

In summary, the following macroscopic damage mechanisms from the drop tests could be observed:

Table 7
Overview of the pre-conditioning of the cells used for the overcharge tests.

Test	Cell damage
1	None, Reference Test
2	Drop on negative pole onto aluminum 50 times
3	Drop on positive pole onto aluminum 50 times
4	Drop on positive pole onto polyurethane until $\Delta R_i > 5m\Omega$
5	Drop on negative pole onto polyurethane until $\Delta R_i > 5m\Omega$

- Relative movement of the jelly roll and deformation of the overhanging separators and anode
- For some cells: ISC due to deformation of overhanging separators and anodes
- Deterioration of contacts in the CID and a resulting increase of ohmic resistance
- For some cells in a small window before cell failure: potential change in current path due to tab damage
- Ultimate high ohmic failure due to contact loss in the CID area

It has to be kept in mind that while there were no hazardous events reported in this study, this might be the case when testing a larger sample size or when testing with even higher loads, which could cause other failure mechanisms. For this reason, even though the battery cells showed a high safety level in the tests, occurring loads and appropriate damping and damage protection should always be taken into account when designing battery packs. This experiment should also not be interpreted as a general comparative study of the robustness of the cells against all types of dynamic loads, as some of the cells that failed early in this test might cope better with dynamic loads with different accelerations than others. For a systematic analysis of CID designs, the reader is referred to Li et al. [42].

The high ohmic cell failure due to contact loss in the CID could also be regarded as a feature that prohibits the further use of heavily damaged cells. However, in some applications, damaged cells are discharged by the BMS, which would be prevented by contact loss and thereby harm the pack safety. Also, manual discharge of damaged cells to allow safe transport and recycling is hindered.

5. Investigation of the impact of dynamic loads on cell safety

While the previous test series confirmed that the primary failure mechanism is high ohmic, CT scans of cells in Section 4.3.1 also revealed that dynamic loads can also result in a significant increase of ohmic resistance and severe deformation of the CID. This might not only affect the electrical behavior of the cell, but also the functionality of the CID and could thereby cause a critical event even days or months after the initial damaging event. To analyze if damages caused by dynamic loads can harm the functionality of the CID of 18650 cells overcharge tests were performed with damaged cells.

5.1. Test setup and performed tests

Therefore new and damaged cells of the type Samsung INR18650 25RM were prepared according to Table 7, with 4 cells overcharged for each variation. These test settings were chosen to investigate if either increase in ohmic resistance or visible damages in CT can harm functionality of the CID. All cells were overcharged with a Gamry Reference 3000 starting from 0% SOC with 1 C (2.5 A) constant current (CC) with a test end criterion of 15 V. As a safety measure, the overcharging was conducted within a self-constructed safety box (255mm x 235mm x 183mm) with a steel case and an integrated pressure relief flap for the case of a thermal event but lacking temperature regulation. Nevertheless, the cell temperature was logged with thermocouples type K.

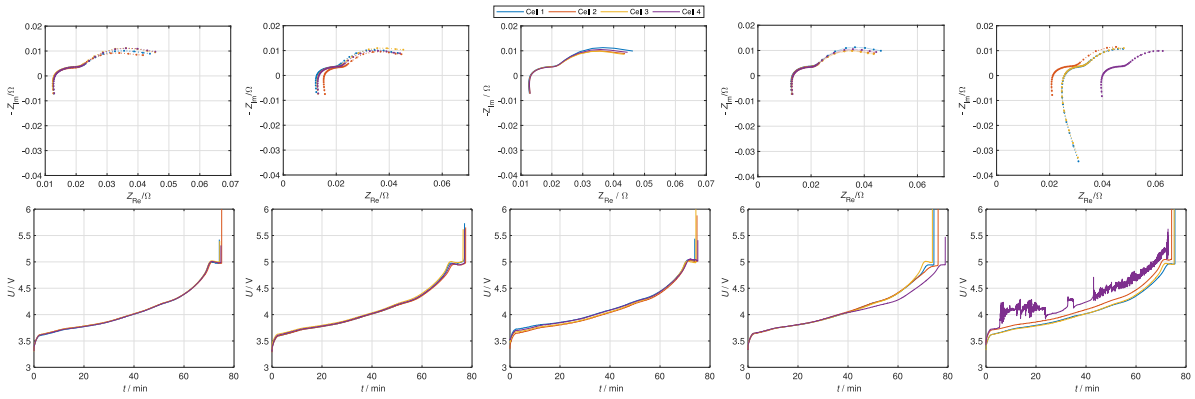

(a) New Cells **(b)** Top Impact, Al. **(c)** Bottom Impact, Al. **(d)** Top Impact, Pol. **(e)** Bottom Impact, Pol.

Fig. 16. Nyquist plots (top) of cells before overcharge tests and voltage over time curves (bottom) during overcharge.

5.2. Results

The Nyquist plots of the reference and the damaged cells are displayed in Fig. 16 after pre-conditioning according to Table 7. For the new cells, deviations in the EIS in the low-frequency range can be attributed to relaxation effects or temperature variations [27–30]. Some of the cells dropped on the positive pole onto aluminum (depicted in Fig. 16(h)), especially cell 2, showed slight increases in ohmic resistance after the drops. The cells dropped with their negative pole onto aluminum (depicted in Fig. 16(i)) showed very little change. For the cells dropped on the positive pole onto polyurethane (depicted in Fig. 16(j)), three of the cells showed changes in their inductive behavior, as shown before, and only one changes in the real part of the impedance. Two cells dropped onto their negative pole (depicted in Fig. 16(k)) show the same behavior and cell 4 shows an increase of ohmic resistance far beyond the minimal requirement of resistance increase but was tested as an example for severe damage anyway.

The conduced overcharge tests showed that the CID consistently prevents thermal events by interrupting the current path. While none of the cells exhibited a thermal runaway, for the 2nd cell with the drop on the positive pole onto the aluminum surface, electrolyte leakage was observed shortly after the triggering of the CID. While the other cells did not show any electrolyte leakage in a liquid form, there was still the smell of electrolyte noticeable in the test chamber, which indicates gaseous electrolyte leakage. Due to their toxicity and the high potential of a hazardous event, no CT or Post Mortem analysis could be performed on these cells.

During the overcharge tests, the voltage curve for all cells shows typical stages during overcharge above 4.2 V, as described by Wang et al. and Haung et al. [43,44], from stronger delithiation of the cathode, to a negative potential shift of the anode and related plating, to accelerated oxidation reaction of the electrolyte and the drop at around 5 V, where a structural change of the cathode active materials and strong side reactions between the electrolyte and the anode interface occur. Finally, at around 75 min after the start of the test, the CID interrupts the current path, causing a voltage spike and the end of the experiment.

The depiction of the voltage curve of the reference cells in Fig. 16(g) only shows slight deviations among the overcharge curves. The cells with positive pole impact on aluminum (depicted in Fig. 16(h)), which results in intense deformation of the CID, show more distinct deviations, yet the CID interrupted the current path within a window of a few minutes. Cells dropped on the negative pole (depicted in Fig. 16(i)) show similar behavior but more substantial differences in the voltage curve at the start of the test. The cells with top impact on polyurethane with small visible deformation in the CID area but significant resistance increase show low initial deviations in their voltage curve but more distinct deviations before the triggering of the CID with several minutes in between their triggering times, as depicted in Fig. 16(j). Significant differences can be observed in the test of the cells with bottom impact onto polyurethane (depicted in Fig. 16(k)), where cell 4, which showed a significant increase of ohmic resistance, shows a voltage curve around 0.2 mV above all other cells with strong fluctuations. Nevertheless, even for this cell, the CID interrupted the current path.

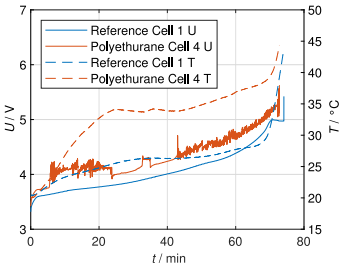

Fig. 17. Temperature and voltage curves for reference cell 1 (Fig. 16(g)) and cell 4 of the test with impact on polyurethane on the negative pole (Fig. 16(k)).

As the test chamber offered no temperature control, the temperature curves recorded show environmental deviations up to 5 °C for many of the tests, there is no unequivocal statement possible if the behavior occurred due to ambient temperature deviations or mechanical cell damage. Merely cell 4 for the drop test on polyurethane with negative pole exhibits a strong correlation in its temperature behavior to the voltage curve, as depicted in Fig. 17.

5.3. Discussion

Despite the severe mechanical damages, the functionality of the CID remained intact in all overcharge tests and reliably prevented a thermal event. With this, it has to be kept in mind, that the chosen voltage test end criterion could be less critical than a criterion that additionally allows CV-charging.

Regarding the electrical behavior, the cells with resistance increase showed deviations from the reference cells in the voltage curves, and, especially cell 4 of the cells with bottom impact onto polyurethane, also in the temperature curve due to ohmic losses. This oscillating behavior in the cell voltage seems to be another sign of loose contact in the CID region, which can not only be found for mechanically damaged cells but also right before the interruption of the current path by the CID as reported in the overheating of 18650 cells by Srinivasan et al. [45]. The observed abnormal thermal and electrical behavior might be an approach for the detection of damaged cells in the BMS, but considering

that the cells with the even stronger deformed CIDs in the drop tests onto aluminum showed significantly fewer variations to the reference cells, it is hardly a reliable indicator of mechanical damage caused by shocks.

6. Conclusion

After the completion of the experimental studies, the results are concluded in the following section.

The literature analysis showed that 18650 cells subjected to dynamic loads may exhibit signs of damage such as an increase in ohmic resistance or imprints of mandrels in current collector tabs, yet known publications do not further investigate the ultimate failure mechanism.

Therefore, as a first experiment to potentially provoke mechanical cell failure, axial shock tests with 1000 repetitions, 300 g acceleration and 6 ms pulse width were conducted on 6 different cell types. It was observed, that under these test conditions, older cell types and types with suboptimal mechanical cell design exhibit damage mechanisms known from literature, such as an increase of ohmic resistance or imprints on the current collector tabs due to a loose jelly roll. Still, no cell failure was reported. On the other hand, state-of-the-art cells showed no changes in EIS nor in CT scans due to their improved cell design.

To investigate if higher accelerations occur beyond these standards and therefore if further testing of the failure mode is practically relevant, acceleration measurements of the impact of commercial power tool battery packs from different heights and on various impact surfaces were executed. For this test series, a drop test bench for modules was used. The results show accelerations above 500 g for a drop test from 0.5 m up to 3000 g for drop tests from 2.0 m, which exceed widely applied battery test standards by far and even go beyond the test conditions in high load standards and strengthened the need for further investigation.

In this further investigation, the failure mode was analyzed using a guided drop test stand for cells. With this test stand, drop tests with 8 different cell types, different orientations, impact surfaces and SOCs were conducted. The results showed increases in ohmic resistance and ultimately high ohmic failure for multiple modern cell types, indicating that cells that did not fail in the tests likely exhibit the same behavior after further loading. Also, the variation of the impact surface resulted in the same failure mechanism. For the cell type used in the SOC variation, self-heating and voltage drainage due to ISCs were reported, but no thermal runaway occurred. The tests indicated, that cells with higher SOCs have a slightly higher resilience against high ohmic failure but show more intense thermal reactions in the case of an ISC.

CT and Post Mortem analysis revealed that the predominant failure mechanism under dynamic loads is the loss of contact in the CID region. For the cell type that exhibited ISCs, their cause was likely the collision of the jelly roll with the bead of the case. The same behavior was not reported for the other modern cells as those still feature somewhat larger anode and separator overhangs, which act as a dampening component. These were possibly reduced for the cell type that showed ISCs to increase its energy content or for electrode balancing. This reveals that for modern battery cells there might be a rising conflict of objectives in cell design between energy density and safety.

Finally, potential implications of mechanical damages on the electrical behavior and the functionality of the CID were investigated by overcharge tests on pre-damaged cells. Despite the severity of the damages and critical electrical and thermal abnormalities that one cell showed, the CID remained functional for all tested cells and prevented thermal runaway.

The conducted tests lead to the conclusion, that while loads in some applications may significantly exceed widely applied standards, state-of-the-art 18650 lithium-ion batteries are very resilient against dynamic loads. Even if a failure occurs, it is likely to be high ohmic and therefore probably not a direct safety issue, yet may harm safety functions on a BMS level. However, a more conclusive statement would require larger sample sizes. In any case, it is recommended that application-specific loads should always be taken into account when designing battery packs and defining test conditions for abuse tests.

Regarding the cell design, the following partly conflicting features for modern cells were derived:

- Tight packaging with dampening components to avoid relative movement.
- Small separator and anode overhang to increase energy density, but big enough overhang to dampen impacts.
- Big enough gaps to compensate for jelly roll swelling to enhance life span, but small gaps between jelly roll and case to prohibit relative movement between jelly roll and case.
- Use of a mandrel to avoid mechanical jelly roll collapse during aging [46] or mandrel-free cell design, as it might damage components within the cell due to relative movement.

Further research should investigate critical loads for 18650 cells by conducting experiments with a high acceleration shock tester and create a relation between failure probability, shock severity (accelerations and pulse widths) and repetitions. Investigations could also include shock tests on aged cells, aging studies of cells after damaging from dynamic loads, more profound testing regarding the influence of the SOC and tests with different cell formats (e.g. 21700). While the cells appear to be very safe, there is little knowledge about potential hazards on module level (e.g. the resilience of cell connectors).

CRediT authorship contribution statement

Markus Spielbauer: Conceptualization, Methodology, Software, Validation, Formal analysis, Investigation, Data curation, Writing – original draft, Writing – review & editing, Visualization. **Philipp Berg:** Conceptualization, Methodology, Resources, Writing – review & editing, Supervision, Funding acquisition. **Jonas Soellner:** Conceptualization, Methodology, Resources, Writing – review & editing. **Julia Peters:** Validation, Investigation, Resources, Data curation, Writing – review & editing. **Florian Schaeufl:** Software, Validation, Investigation, Writing – review & editing. **Christian Rosenmüller:** Validation, Investigation, Writing – review & editing. **Oliver Bohlen:** Conceptualization, Methodology, Resources, Writing – review & editing, Supervision, Project administration, Funding acquisition. **Andreas Jossen:** Conceptualization, Methodology, Resources, Writing – review & editing, Supervision, Project administration, Funding acquisition.

Declaration of competing interest

The authors declare that they have no known competing financial interests or personal relationships that could have appeared to influence the work reported in this paper.

Acknowledgments

Funding from the German Federal Ministry for Economic Affairs and Energy (BMWi) of the project ReVISEDBatt [03ETE004C] and managing by the Projektträger Jülich (PtJ) is gratefully acknowledged. This work was financially supported by the Munich University of Applied Sciences HM and the German Research Foundation (DFG) through the "Open Access Publishing" program. The authors want to express their gratitude to Robert Stanger, Varnim Goyal and Leonard Janczyk from Hilti Entwicklungsgesellschaft mbH for fruitful discussions as well as for supplying the test series with material. The authors also want to thank Prof. Dr. Gregor Feiertag for supporting this project by granting access to the CT scanner.

Appendix A. Abbreviations

See Table A.1.

Table A.1
Abbreviations.

BMS	Battery Management System
CID	Current Interruptive Device
EIS	Electrochemical Impedance Spectroscopy
ISC	Internal Short Circuit
CC	Constant Current
CT	Computed Tomography
OCV	Open circuit voltage
SOC	State of Charge
SOH	State of Health

Appendix B. Acceleration measurements of module drop tests

See Fig. B.18.

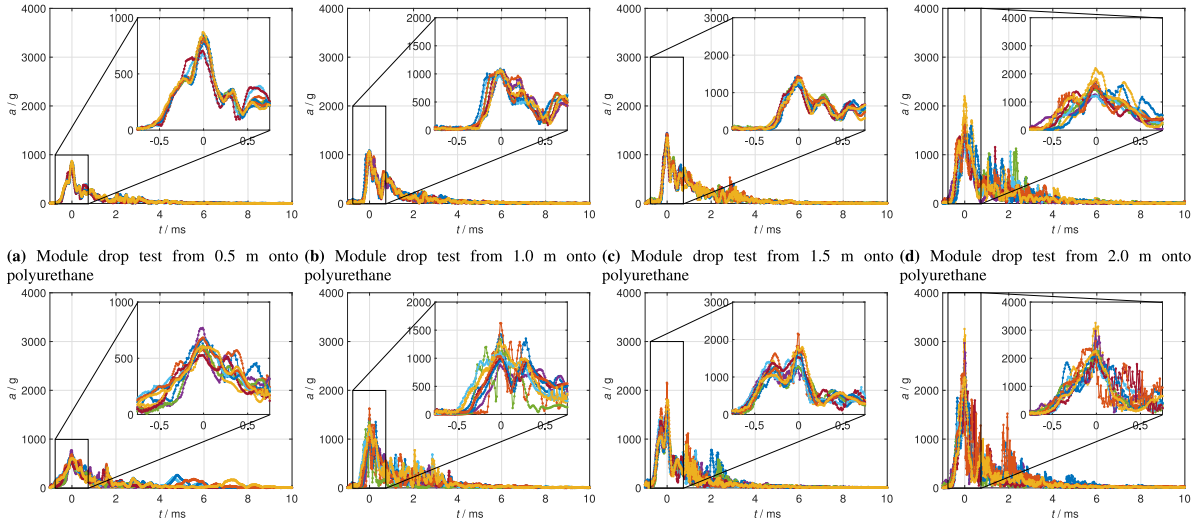

(a) Module drop test from 0.5 m onto polyurethane **(b)** Module drop test from 1.0 m onto polyurethane **(c)** Module drop test from 1.5 m onto polyurethane **(d)** Module drop test from 2.0 m onto polyurethane

(e) Module drop test from 0.5 m onto aluminum **(f)** Module drop test from 1.0 m onto aluminum **(g)** Module drop test from 1.5 m onto aluminum **(h)** Module drop test from 2.0 m onto aluminum

Fig. B.18. Drop tests of a commercial power tool battery module onto different impact surfaces from various heights.

Appendix C. Impedance measurements of a drop test of the Samsung INR18650-35E

See Fig. C.19.

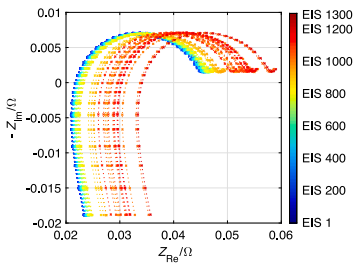

Fig. C.19. Nyquist Plot of a preconducted drop test on a Samsung INR18650-35E onto polyurethane with an EIS measurement every 20 drops.

Appendix D. CT scans of drop tests on aluminum

See Fig. D.20.

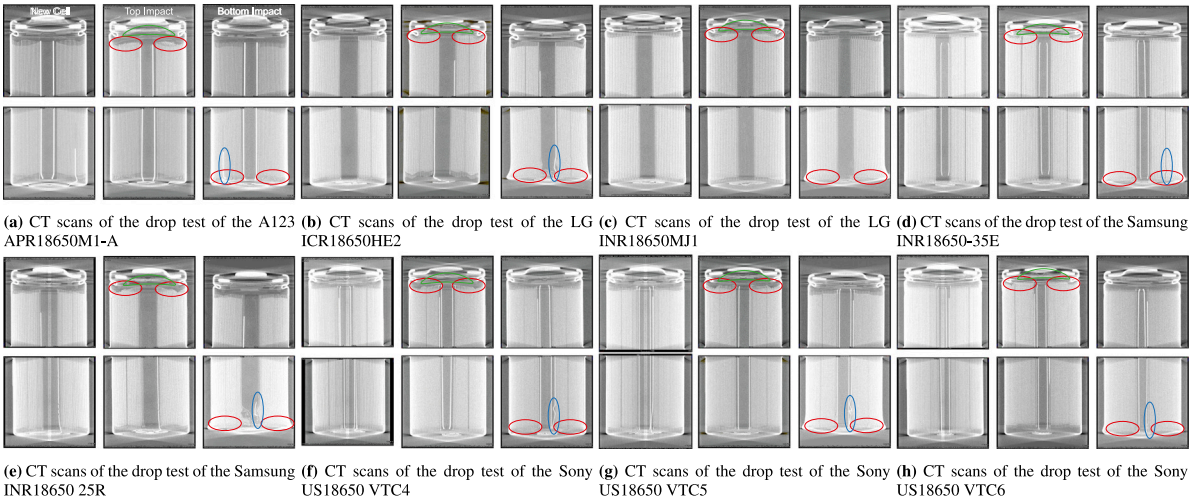

(a) CT scans of the drop test of the A123 APR18650M1-A **(b)** CT scans of the drop test of the LG ICR18650HE2 **(c)** CT scans of the drop test of the LG INR18650MJ1 **(d)** CT scans of the drop test of the Samsung INR18650-35E

(e) CT scans of the drop test of the Samsung INR18650 25R **(f)** CT scans of the drop test of the Sony US18650 VTC4 **(g)** CT scans of the drop test of the Sony US18650 VTC5 **(h)** CT scans of the drop test of the Sony US18650 VTC6

Fig. D.20. CT scans of drop tests on aluminum. Each time a new cell, a cell with top impact and a cell with bottom impact are displayed. Deformation of overhanging anode (red), the CID (green) and current collectors (blue) can be observed. (For interpretation of the references to color in this figure legend, the reader is referred to the web version of this article.)

Appendix E. Anode overhang lengths

See Table E.8.

Table E.8
Lengths of anode overhangs at the positive pole of cells used in the drop test series.

Cell Type	A123 APR18650M1-A	LG ICR18650HE2	LG INR18650MJ1	Samsung INR18650-35E	Samsung INR18650 25RM	Sony/Murata Konion US18650 VTC4	Sony/Murata Konion US18650 VTC5	Sony/Murata Konion US18650 VTC6
Min. Overhang Length in mm	0.31	1.06	0.65	0.66	0.51	0.43	0.67	0.38
Max. Overhang Length in mm	1.26	1.26	0.83	0.76	0.65	0.68	0.98	0.54

References

[1] V. Ruiz, A. Pfrang, A. Kriston, N. Omar, P. van den Bossche, L. Boon-Brett, A review of international abuse testing standards and regulations for lithium ion batteries in electric and hybrid electric vehicles, Renew. Sustain. Energy Rev. 81 (2018) 1427–1452, http://dx.doi.org/10.1016/j.rser.2017.05.195.

[2] S. Arora, W. Shen, A. Kapoor, Review of mechanical design and strategic placement technique of a robust battery pack for electric vehicles, Renew. Sustain. Energy Rev. 60 (2016) 1319–1331, http://dx.doi.org/10.1016/j.rser.2016.03.013.

[3] UN/ECE-R100.02, Regulation no 100 of the economic commission for europe of the united nations (UNECE) — Uniform provisions concerning the approval of vehicles with regard to specific requirements for the electric power train, 2015.

[4] IEC62660-2, Secondary lithium-ion cells for the propulsion of electric road vehicles - part 2: Reliability and abuse testing, 2018.

[5] ISO16750-3, Road vehicles — Environmental conditions and testing for electrical and electronic equipment — Part 3: Mechanical loads, 2013.

[6] UL 2580, Batteries for use in electric vehicles, 2013.

[7] UL1642, Standard for safety-lithium batteries, 2012.

[8] SAE J2464, Electric and hybrid electric vehicle rechargeable energy storage system (RESS) safety and abuse testing, 2010.

[9] SAE J2929, Safety standard for electric and hybrid vehicle propulsion battery systems utilizing lithium-based rechargeable cells, 2013.

[10] UN38.3, Transport of dangerous goods: Manual of tests and criteria Fifth revised edition 43–51.

[11] MIL-STD-202G, Department of defense test method standard electronical and electrical component parts, 2002.

[12] NASA/TM-2009-215751, Guidelines on lithium-ion battery use in space applications, 2009.

[13] IEC 60068-2-27, Environmental testing - part 2-27: Tests - test ea and guidance: Shock, 2008.

[14] QC/T 743, Lithium-ion batteries for electric vehicles, 2006.

[15] FreedomCAR, Electrical energy storage system abuse test manual for electric and hybrid electric vehicle applications, 2006.

[16] MIL-STD-810H, Department of defense test method standard: Environmental engineering considerations and laboratory tests, 2019.

[17] G. Kjell, J.F. Lang, Comparing different vibration tests proposed for li-ion batteries with vibration measurement in an electric vehicle, in: EVS27 International Battery, Hybrid and Fuel Cell Electric Vehicle Symposium, 2013.

[18] J.F. Lang, G. Kjell, Comparing vibration measurements in an electric vehicle with standard vibration requirements for Li-ion batteries using power spectral density analysis, Int. J. Electr. Hybrid Veh. 7 (3) (2015) 272, http://dx.doi.org/10.1504/IJEHV.2015.071640.

[19] M.J. Brand, S.F. Schuster, T. Bach, E. Fleder, M. Stelz, S. Gläser, J. Müller, G. Sextl, A. Jossen, Effects of vibrations and shocks on lithium-ion cells, J. Power Sources 288 (2015) 62–69, http://dx.doi.org/10.1016/j.jpowsour.2015.04.107.

[20] T. Tsujikawa, K. Yabuta, M. Arakawa, K. Hayashi, Safety of large-capacity lithium-ion battery and evaluation of battery system for telecommunications, J. Power Sources 244 (2013) 11–16, http://dx.doi.org/10.1016/j.jpowsour.2013.01.155.

[21] F. Ebert, G. Sextl, M. Lienkamp, Influence of dynamic mechanical stress on lithiumion-battery aging, in: 6th Conference on Future Automotive Technology, 2017.

[22] J. Hooper, J. Marco, G. Chouchelamane, C. Lyness, Vibration durability testing of nickel manganese cobalt oxide (NMC) Lithium-Ion 18,650 battery cells, Energies 9 (1) (2016) 52, http://dx.doi.org/10.3390/en9010052.

[23] T. Bruen, J. Hooper, J. Marco, M. Gama, G. Chouchelamane, Analysis of a battery management system (BMS) control strategy for vibration aged nickel manganese cobalt oxide (NMC) lithium-ion 18650 battery cells, Energies 9 (4) (2016) 255, http://dx.doi.org/10.3390/en9040255.

[24] J.M. Hooper, J. Marco, G.H. Chouchelamane, J.S. Chevalier, D. Williams, Multi-axis vibration durability testing of lithium ion 18650 NCA cylindrical cells, J. Energy Storage 15 (2018) 103–123, http://dx.doi.org/10.1016/j.est.2017.11.006.

[25] L. Somerville, J. Hooper, J. Marco, A. McGordon, C. Lyness, M. Walker, P. Jennings, Impact of vibration on the surface film of lithium-ion cells, Energies 10 (6) (2017) 741, http://dx.doi.org/10.3390/en10060741.

[26] P. Berg, M. Spielbauer, M. Tillinger, M. Merkel, M. Schoenfuss, O. Bohlen, A. Jossen, Durability of lithium-ion 18650 cells under random vibration load with respect to the inner cell design, J. Energy Storage 31 (2020) 101499, http://dx.doi.org/10.1016/j.est.2020.101499.

[27] C.T. Love, M.B. Virji, R.E. Rocheleau, K.E. Swider-Lyons, State-of-health monitoring of 18650 4S packs with a single-point impedance diagnostic, J. Power Sources 266 (2014) 512–519, http://dx.doi.org/10.1016/j.jpowsour.2014.05.033.
[28] C. Love, M. Dubarry, T. Reshetenko, A. Devie, N. Spinner, K. Swider-Lyons, R. Rocheleau, Lithium-ion cell fault detection by single-point impedance diagnostic and degradation mechanism validation for series-wired batteries cycled at 0 °C, Energies 11 (4) (2018) 834, http://dx.doi.org/10.3390/en11040834.
[29] J.P. Schmidt, S. Arnold, A. Loges, D. Werner, T. Wetzel, E. Ivers-Tiffée, Measurement of the internal cell temperature via impedance: Evaluation and application of a new method, J. Power Sources 243 (2013) 110–117, http://dx.doi.org/10.1016/j.jpowsour.2013.06.013.
[30] H.P.G.J. Beelen, L.H.J. Raijmakers, M.C.F. Donkers, P.H.L. Notten, H.J. Bergveld, A comparison and accuracy analysis of impedance-based temperature estimation methods for li-ion batteries, Appl. Energy 175 (5) (2016) 128–140, http://dx.doi.org/10.1016/j.apenergy.2016.04.103.
[31] A. Barai, G.H. Chouchelamane, Y. Guo, A. McGordon, P. Jennings, A study on the impact of lithium-ion cell relaxation on electrochemical impedance spectroscopy, J. Power Sources 280 (2015) 74–80, http://dx.doi.org/10.1016/j.jpowsour.2015.01.097.
[32] F.M. Kindermann, A. Noel, S.V. Erhard, A. Jossen, Long-term equalization effects in li-ion batteries due to local state of charge inhomogeneities and their impact on impedance measurements, Electrochim. Acta 185 (2015) 107–116, http://dx.doi.org/10.1016/j.electacta.2015.10.108.
[33] J. Park, S. Kalnaus, S. Han, Y.K. Lee, G.B. Less, N.J. Dudney, C. Daniel, A.M. Sastry, In situ atomic force microscopy studies on lithium (de)intercalation-induced morphology changes in LixCoO2 micro-machined thin film electrodes, J. Power Sources 222 (2013) 417–425, http://dx.doi.org/10.1016/j.jpowsour.2012.09.017.
[34] B. Rieger, S. Schlueter, S.V. Erhard, J. Schmalz, G. Reinhart, A. Jossen, Multi-scale investigation of thickness changes in a commercial pouch type lithium-ion battery, J. Energy Storage 6 (2016) 213–221, http://dx.doi.org/10.1016/j.est.2016.01.006.
[35] K.-Y. Oh, J.B. Siegel, L. Secondo, S.U. Kim, N.A. Samad, J. Qin, D. Anderson, K. Garikipati, A. Knobloch, B.I. Epureanu, C.W. Monroe, A. Stefanopoulou, Rate dependence of swelling in lithium-ion cells, J. Power Sources 267 (2014) 197–202, http://dx.doi.org/10.1016/j.jpowsour.2014.05.039.
[36] T. Kuttner, Praxiswissen Schwingungsmesstechnik, Springer Fachmedien, Wiesbaden, 2015.
[37] S.F. Schuster, M.J. Brand, P. Berg, M. Gleissenberger, A. Jossen, Lithium-ion cell-to-cell variation during battery electric vehicle operation, J. Power Sources 297 (2015) 242–251, http://dx.doi.org/10.1016/J.JPOWSOUR.2015.08.001.
[38] K. Rumpf, M. Naumann, A. Jossen, Experimental investigation of parametric cell-to-cell variation and correlation based on 1100 commercial lithium-ion cells, J. Energy Storage 14 (2017) 224–243, http://dx.doi.org/10.1016/j.est.2017.09.010.
[39] M. Raffler, A. Sevarin, C. Ellersdorfer, S.F. Heindl, C. Breitfuss, W. Sinz, Finite element model approach of a cylindrical lithium ion battery cell with a focus on minimization of the computational effort and short circuit prediction, J. Power Sources 360 (2017) 605–617, http://dx.doi.org/10.1016/j.jpowsour.2017.06.028.
[40] J. Zhu, X. Zhang, E. Sahraei, T. Wierzbicki, Deformation and failure mechanisms of 18650 battery cells under axial compression, J. Power Sources 336 (2016) 332–340, http://dx.doi.org/10.1016/j.jpowsour.2016.10.064.
[41] P.J. Osswald, S.V. Erhard, A. Noel, P. Keil, F.M. Kindermann, H. Hoster, A. Jossen, Current density distribution in cylindrical li-ion cells during impedance measurements, J. Power Sources 314 (2016) 93–101, http://dx.doi.org/10.1016/j.jpowsour.2016.02.070.
[42] W. Li, K.R. Crompton, C. Hacker, J.K. Ostanek, Comparison of current interrupt device and vent design for 18650 format lithium-ion battery caps, J. Energy Storage 32 (2020) 101890, http://dx.doi.org/10.1016/j.est.2020.101890.
[43] L. Huang, Z. Zhang, Z. Wang, L. Zhang, X. Zhu, D.D. Dorrell, Thermal runaway behavior during overcharge for large-format lithium-ion batteries with different packaging patterns, J. Energy Storage 25 (2019) 100811, http://dx.doi.org/10.1016/j.est.2019.100811.
[44] Q. Wang, P. Ping, X. Zhao, G. Chu, J. Sun, C. Chen, Thermal runaway caused fire and explosion of lithium ion battery, J. Power Sources 208 (2012) 210–224, http://dx.doi.org/10.1016/j.jpowsour.2012.02.038.
[45] R. Srinivasan, M.E. Thomas, M.B. Airola, B.G. Carkhuff, L. Frizzell-Makowski, H. Alkandry, J.G. Reuster, H.N. Oguz, P.W. Green, J. La Favors, L.J. Currano, P.A. Demirev, Preventing cell-to-cell propagation of thermal runaway in lithium-ion batteries, J. Electrochem. Soc. 167 (2) (2020) 020559, http://dx.doi.org/10.1149/1945-7111/ab6ff0.
[46] A. Pfrang, A. Kersys, A. Kriston, D.U. Sauer, C. Rahe, S. Käbitz, E. Figgemeier, Geometrical inhomogeneities as cause of mechanical failure in commercial 18650 lithium ion cells, J. Electrochem. Soc. 166 (15) (2019) A3745–A3752, http://dx.doi.org/10.1149/2.0551914jes.